JACS
JOURNAL OF THE AMERICAN CHEMICAL SOCIETY

ARTICLE

pubs.acs.org/JACS

Dual Path Mechanism in the Thermal Reduction of Graphene Oxide

Rosanna Larciprete,[*,†] Stefano Fabris,[‡,§] Tao Sun,[‡,§] Paolo Lacovig,[‖] Alessandro Baraldi,[⊥,#] and
Silvano Lizzit[*,‖]

[†]CNR-Institute for Complex Systems, via Fosso del Cavaliere 100, I-00133 Roma, Italy
[‡]CNR-IOM DEMOCRITOS, Theory@Elettra group, S.S. 14 km 163.5, I-34149 Trieste, Italy
[§]SISSA — Scuola Internazionale Superiore di Studi Avanzati, via Bonomea 265, I-34136 Trieste, Italy
[‖]Sincrotrone Trieste S.C.p.A., Strada Statale 14 Km 163.5, I-34149 Trieste, Italy
[⊥]Physics Department and CENMAT, University of Trieste, Via Valerio 2, I-34127 Trieste, Italy
[#]Laboratorio TASC CNR-IOM, S.S. 14 Km 163.5, I-34149 Trieste, Italy

S *Supporting Information*

ABSTRACT:

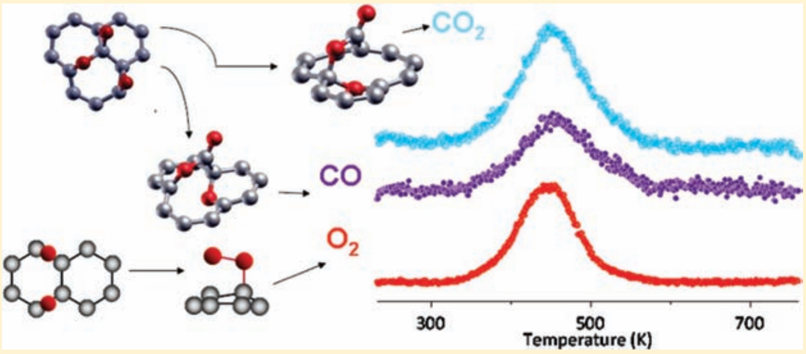

Graphene is easily produced by thermally reducing graphene oxide. However, defect formation in the C network during deoxygenation compromises the charge carrier mobility in the reduced material. Understanding the mechanisms of the thermal reactions is essential for defining alternative routes able to limit the density of defects generated by carbon evolution. Here, we identify a dual path mechanism in the thermal reduction of graphene oxide driven by the oxygen coverage: at low surface density, the O atoms adsorbed as epoxy groups evolve as O_2 leaving the C network unmodified. At higher coverage, the formation of other O-containing species opens competing reaction channels, which consume the C backbone. We combined spectroscopic tools and ab initio calculations to probe the species residing on the surface and those released in the gas phase during heating and to identify reaction pathways and rate-limiting steps. Our results illuminate the current puzzling scenario of the low temperature gasification of graphene oxide.

INTRODUCTION

The possibility of efficiently reducing graphene oxide (GO) while maintaining optimal transport properties is a challenging issue that needs to be faced in view of widening the versatility of graphene in electronics and optoelectronics.[1−3] The property of GO of being solution processable and easy to handle is provided by O atoms attached to the graphene scaffold in several oxidizing groups, with a relative abundance controlled by the preparation methods.[2,4−6] Graphene oxide is an insulating material, and progressive elimination of oxygen results in a gradual increase of the electronic mobility.[7−10] However, the transport properties of reduced GO are far from being comparable to those of ideal dopant-free graphene because the sp^2 conjugation is only partially retrieved.[11,12] Actually, materials resulting from the oxo-reduction cycle present severe limitations due to the generation of topological defects and C vacancies[13,14] and to the permanent inclusion of foreign atoms in the graphene lattice.[11,12,15,16]

Currently, GO is deoxygenated via chemical[5,17,18] as well as thermal routes.[8,10,19−21] In this context, the appeal of using thermal processing is reinforced by the possibility to remove oxygen with submicrometric lateral resolution by handling nanosized heat sources.[22,23] It is well assessed that thermal reduction of GO occurs around 450 K,[8,10,19] with the release of H_2O, CO, and CO_2 in the gas phase. The latter process originates vacancies in the graphene basal plane and consumes the edges. Thermal desorption of molecular oxygen is instead either not detected[19,21] or present only in traces.[10] Moreover, the GO mass

Received: June 4, 2011
Published: August 16, 2011

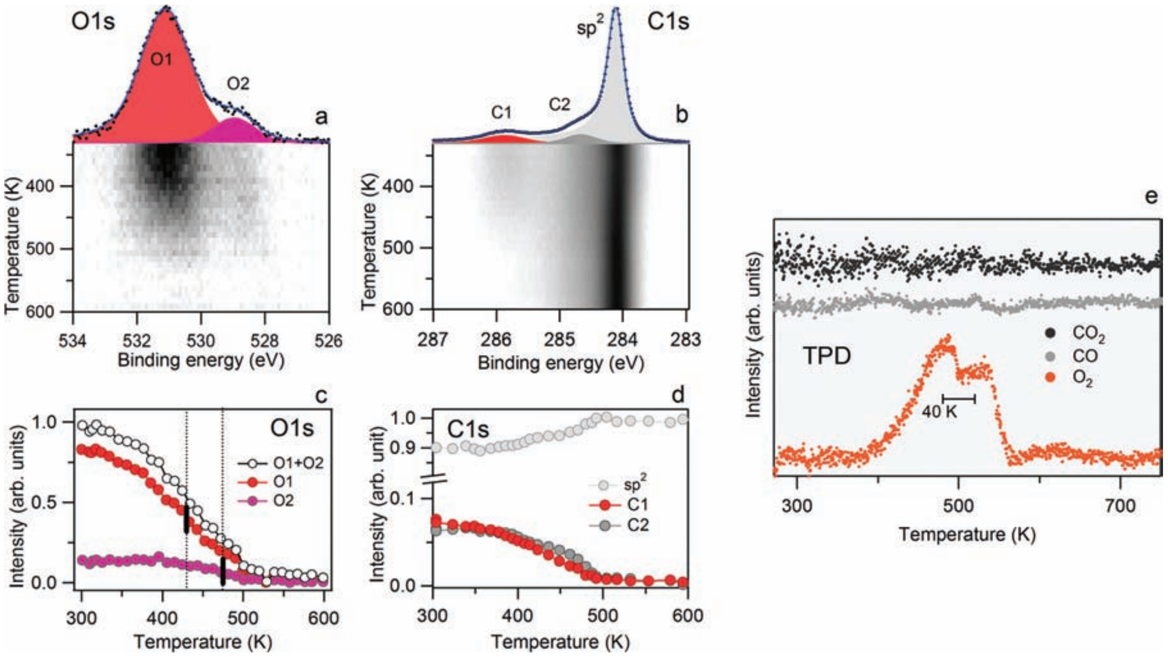

Figure 1. Surface composition and thermal annealing of graphene with low O coverage. (a,b) Top: O1s and C1s core level spectra measured on graphene/Ir(111) with an oxygen coverage $\theta = 0.03$ ML. The best fit curves and the spectral components are indicated by the blue lines and the colored peaks. Bottom: Coded density plots of the O1s and C1s spectral intensities versus temperature. The C1s image is saturated to highlight the evolution of the minor spectral components. (c,d) O1s (c) and C1s (d) component intensities versus temperature measured at a rate of 0.2 K/s. The two bars in (c) mark the inflection points of the O1 and O2 curves. (e) TPD curves measured during annealing of the sample at a rate of 2 K/s. The curves are background subtracted and vertically shifted for clarity.

loss attributed indistinctly to the decomposition of functional groups anchored directly to GO or attached to oxidized debris non covalently bonded to GO[5,10,12,19,20] still needs to be clarified.

Carbon gasification during GO reduction is determined by the nature and concentration of the oxidizing groups and the manifold of surface reactions thermally activated that compete with each other. This scenario is made rather complex by the intriguing chemical composition of GO that contains epoxy and hydroxyl groups on the basal plane as well as carbonyls, carboxyls, ethers, quinones, lactols, and phenols attached at vacancy and edge sites.[24−27] For OH groups as well as for the oxidizing species attached to vacancies and edges, the thermal behavior is somehow assessed and a stability scale commonly accepted.[28,29] On the contrary, for epoxy groups the analogous information concerning surface diffusion, stability, reaction routes, and desorption temperature is quite vague. This is likely because the reduction of graphitic C is traditionally investigated on materials oxidized at temperatures above 500−600 K[30,32] that appear too high for the retention of epoxy oxygens, which have been reported to desorb below 400 K.[24,33] However, basal plane O atoms have been often theoretically predicted[34−38] to be reactive agents capable of promoting the formation of more complex oxidized structures and of catalyzing surface reactions, and might represent the key species in the low temperature gasification of GO.

Here, we identify a dual path mechanism for the reduction of oxidized graphene governed by the coverage of oxygen atoms. The thermal reduction of graphene oxidized by a low density of epoxy groups proceeds by releasing solely molecular oxygen via a cycloaddition reaction from epoxy−epoxy pairs. It is the formation of ether−epoxy pairs at high O coverage that promotes the elimination of CO/CO$_2$ mixtures, thus determining surface defects and C loss. We demonstrate that the competing surface reactions leading to molecular oxygen and CO/CO$_2$ evolution are always assisted by epoxide diffusion and have comparable energy barriers.

We combined high-resolution fast X-ray photoelectron spectroscopy (XPS) with synchrotron radiation and temperature programmed desorption (TPD) with numerical modeling based on Density Functional Theory (DFT) to reveal the species residing on oxidized graphene and released in the gas phase at different temperatures, to address the energetics and diffusion of the surface groups, and to identify the reaction pathways and the rate-limiting steps for the reduction. The oxidized graphene was prepared by dosing oxygen atoms onto a graphene layer grown on the Ir(111) surface. The reason of this choice is 2-fold: (i) the graphene layer supported on Ir(111) is highly ordered with a very low concentration of defects,[39] which may drastically affect the oxidation/deoxidation processes and, (ii) due to the very weak interaction with the underlying substrate, graphene can be seen as almost freestanding.[40,41] Indeed, the lattice mismatch between graphene and Ir(111) gives rise to the formation of a moiré periodic corrugation of the carbon layer, where graphene regions almost completely detached from the substrate coexist with regions that are closer to the Ir surface, thus feeling a slightly stronger interaction. We find that the thermal behavior of the majority of the O-carrying surface species is not affected by this corrugation that, as shown below, is just reflected in the formation of a small amount of C−O bonds most probably residing in the depressions of the graphene layer.

■ RESULTS AND DISCUSSION

Low O Coverage. The graphene layer was exposed to controlled doses of oxygen atoms at room temperature, leading to a

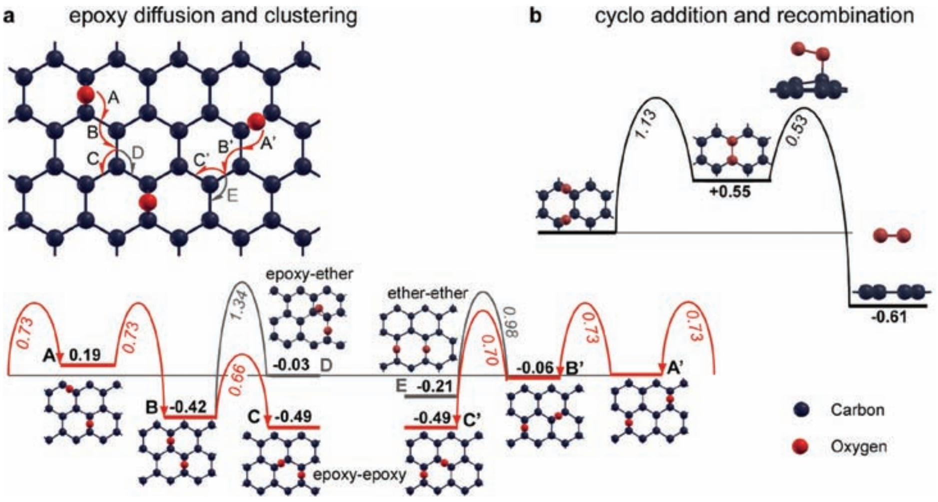

Figure 2. Calculated minimum energy paths for epoxy diffusion, clustering, and recombination to molecular oxygen. (a) Relative energy of the most stable structures involving epoxy pairs as well as calculated activation energies for epoxy diffusion and formation of epoxy−epoxy (C, C′), epoxy−ether (D), and ether−ether (E) groups. (b) Calculated minimum energy path for the recombination of an epoxy−epoxy pair to molecular oxygen via a cycloaddition reaction. All energy values are in eV.

coverage of $\theta = 0.03$ monolayers (ML). With respect to the clean graphene on Ir(111) surface, which shows a single sp^2 peak (284.14 eV)[41] in the C1s spectrum and the components due to bulk (Ir_B, 60.84 eV) and first layer Ir atoms (Ir_S, 60.32 eV) in the $Ir4f_{7/2}$ spectrum[41] (Figure S1), new features in the XPS spectra are observed after oxidation (Figures 1a,b). The oxygen atoms induce a dominant O1 component (531.1 eV) in the O1s spectrum and a C1 component (285.8 eV) in the C1s spectrum, both due to the formation of epoxy structures.[42−44] The appearance of the components C2 (284.6 eV) in the C1s and of a new component (60.66 eV) in the $Ir4f_{7/2}$ spectrum (Figure S1) supports the emergence of a C−Ir interaction induced by the adsorption of O atoms on graphene.[44] Moreover, the Ir-supported graphene shows novel O adspecies, so far unreported in oxidized graphite or carbon nanotubes, originating the component O2 (528.8 eV) in the O1s spectrum.

The thermal evolution of the C1s and O1s spectra (Figures 1a−d) acquired while heating the oxidized graphene described above sets the onset for reduction at $T \approx 350$ K. This temperature activates the O desorption from the epoxy groups only, as shown by the decrease of the O1 and C1 intensities at ∼350 K, whereas the O2 and C2 peaks start to decrease at ∼400 K. In particular, the curves relative to O1 and O2 exhibit inflection points, maximal desorption rates, at T_{max} = 430 and 475 K, 45 K apart from each other (Figure 1c). The similarity between the desorption temperatures measured for O1 and O2 disproves the recent attribution of the O2 component to O atoms intercalated between the metal substrate and the graphene layer,[44] as O atoms bonded to Ir(111), even if under the graphene cover, should desorb at a temperature a few hundred kelvin higher than that measured for O2.[46] Moreover, the high perfectness of graphene grown on Ir(111), with a low density of defects or vacancies, which are the only places where the oxygen atoms could intercalate to bind to the metal substrate, further excludes this attribution. Instead, the slightly higher thermal stability of the O adatoms originating O2 can reasonably derive from the availability of adsorption sites where the oxygen atoms can bind more strongly than the epoxy species generating O1. We guess that the O2 component belongs to the oxygen atoms that are adsorbed in the moiré regions closer to the metal substrate in analogy with the H adsorbate.[45]

No oxygen adatom is detected above 520 K. At these temperatures, the C1s and $Ir4f_{7/2}$ spectra resemble those of pristine graphene, therefore showing that after complete reduction the C atoms recover the full sp^2 hybridization and the bonding with the Ir support is lost. In addition, the integral area of the C1s peak is comparable to the one measured before oxidation, indicating the lack of C loss during the oxidation−reduction cycle.

The decrease in the O-related XPS peaks between 350 and 520 K correlates with the TPD curves measured between room temperature and 750 K (Figure 1e). The data relative to masses 28 (CO), 32 (O_2), and 44 (CO_2) demonstrate that only molecular oxygen is released by the oxidized graphene, whereas the quantity of CO and CO_2 remains below the detection limit, in agreement with the integrity of the reduced graphene indicated by XPS. These results unambiguously prove that O atoms can be reversibly adsorbed and desorbed from the basal plane of perfect graphene layers without leading to vacancy formation in the C network.

The two desorption rate maxima appearing in the O_2 TPD curve at T_{max} = 480 and ∼520 K with a relative shift of ∼40 K can be attributed to the desorption of the two species represented by the O1 and O2 components, which exhibit a similar separation between their T_{max} values (Figure 1c). Note that the upshift of about 50 K of the maximal desorption rates shown by the TPD curves with respect to those derived from the XPS data is due to the different heating rates[47] used during the XPS (0.2 K/s) and TPD (2 K/s) experiments, which were suitably selected to optimize the signal-to-noise ratio for each technique. From the T_{max} values of 480 and 520 K, we estimate desorption energies of 1.21 ± 0.02 and 1.33 ± 0.02 eV when assuming a second-order desorption and a pre-exponential factor of 10^{13} s^{-1}.[45]

Our DFT calculations show that the desorption of molecular oxygen is governed by a cycloaddition reaction between two epoxy groups and is mediated by epoxy group diffusion. The calculated barrier for the diffusion of an epoxy O atom on graphene is 0.73 eV (Figure 2a).[38] According to the transition state theory (assuming a prefactor of 10^{13} s^{-1} $T = 350$ K), this

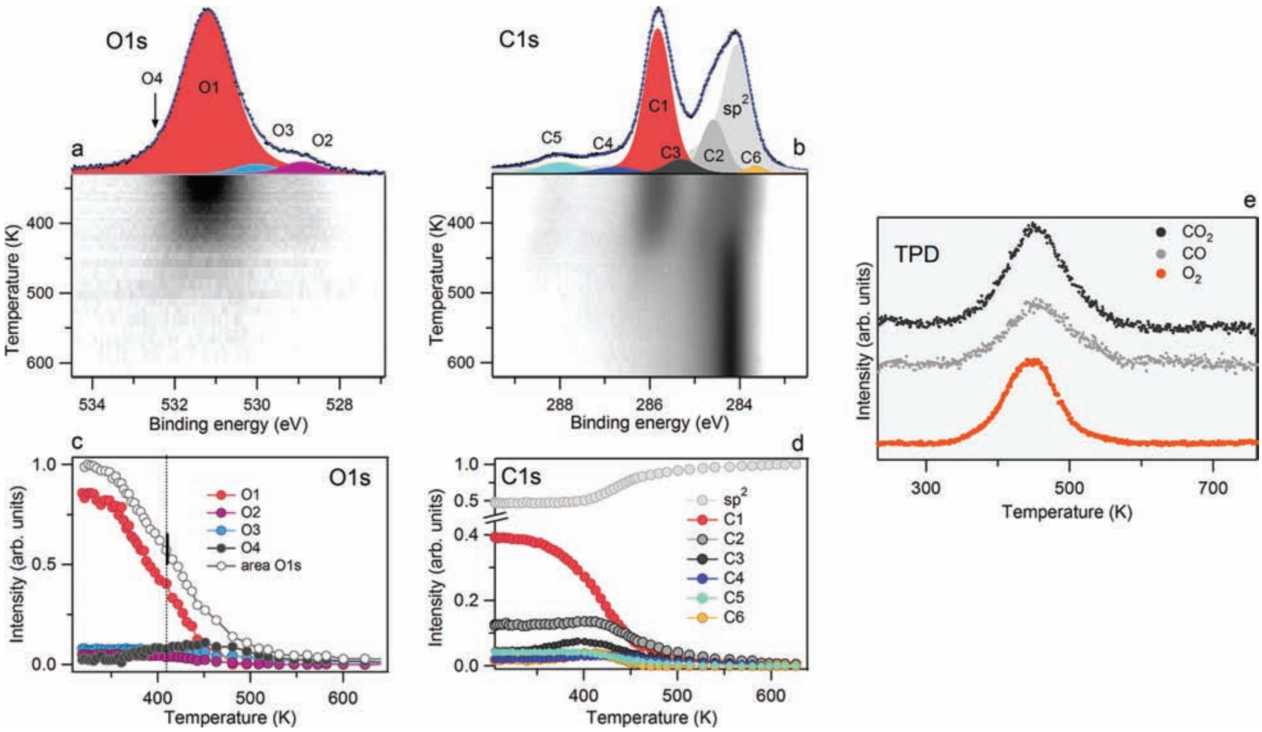

Figure 3. Surface composition and thermal annealing of graphene with high O coverage. (a,b) Top: O1s and C1s core level spectra measured on graphene/Ir(111) with an oxygen coverage $\theta = 0.25$ ML. The best fit curves and the spectral components are indicated by the blue lines and the colored peaks. The component C3, C4, and C5 are attributed to ethers, semiquinones, and lactones, respectively, whereas the weak peak C6 is due to C atoms neighboring lattice vacancies. In the O1s spectrum, the weak component O3 indicates C═O double bonds, whereas the component O4 at 532.4 eV due to ethers cannot be disentangled from the intense O1 peak and becomes visible only above 350 K after epoxy desorption (Figure S2). Bottom: Coded density plots of the O1s and C1s spectral intensities versus temperature. The C1s image is saturated to highlight the evolution of the minor spectral components. (c,d) O1s (c) and C1s (d) component intensities versus temperature measured at a rate of 0.2 K/s. The bar in (c) marks the inflection point of the curve relative to the O1s area. (e) TPD curves measured during the thermal annealing of the sample illustrated above at a rate of 2 K/s. The curves are background subtracted and vertically shifted for clarity.

activation energy corresponds to rates of about 10^2 s^{-1}, and hence the O adsorbates are mobile in the relevant T range.

In these conditions, the calculations predict the clustering of the epoxy groups in second-nearest neighbor configurations (C and C′ in Figure 2a), with an energy gain of almost 0.5 eV. The recombination of these epoxy−epoxy pairs into adsorbed molecular oxygen proceeds via a cycloaddition reaction and requires an activation energy of 1.13 eV (Figure 2b),[48] in close agreement with the experimental value of 1.21 eV resulting from the TPD data. The adsorbed oxygen molecules then desorb to the gas phase with a barrier of just 0.53 eV. Note that the next- and third-nearest neighbor configurations of O adatoms (epoxy−ether and ether−ether, D and E in Figure 2a, respectively) cannot be formed by epoxide diffusion, because this requires activation energies (∼1.3 eV) larger than that needed for the epoxide recombination. We have also verified that O_2 desorption from the cycloaddition intermediate is energetically preferred over its surface rearrangement into a stable pair of semiquinones (Figure S3).

High O Coverage. The O1s and C1s spectra measured on the graphene surface with an oxygen coverage $\theta = 0.25$ ML are shown in Figure 3a and b. Epoxy groups, which are still largely dominating, are accompanied by a low concentration (∼8%) of C atoms forming single, double, and triple bonds with O atoms. We assign the component C3 (285.3 eV) to ethers,[49] whereas the components C4 (286.8 eV) and C5 (288.0 eV) can be attributed to C atoms forming double (quinones) and triple (lactones) bonds with O atoms, respectively.[43] Carbon vacancies originate the small C6 component (283.6 eV) partially responsible for the broadening of the main sp^2 peak.[42] Double C═O bonds produce the O3 component (530.0 eV) in the O1s spectrum, whereas the presence of ethers that generate the component O4 around 532.4 eV[44] (Figure S2) cannot be disentangled from the intense O1 component.

The thermal evolution of the C1s and O1s spectra shows that, similarly to the previous low coverage case, epoxide reduction is activated at ∼300−350 K and is completed below 550 K (Figure 3a−d). A residual quantity of O is still detected at 500 K in the form of ether and semiquinone and is reduced after annealing to $T > 640$ K (Figure S2). The comparison between the C1s spectral intensities measured on pristine and reduced graphene shows that 10−15% of C atoms are lost during the oxidation−desorption cycle. This is at variance with graphene oxidized only with epoxy groups, which are reversibly reduced to the pristine defect-free graphene.

The TPD curves reported in Figure 3e show that the desorption of molecular oxygen between 350 and 550 K is paralleled by the removal of comparable quantities of CO and CO_2 . Hence, the kinetics of the three reactions leading to O_2, CO, and CO_2 should be controlled by rate-limiting steps having similar activation energies. Desorption energies of 1.19−1.21 eV are estimated for the three molecules from the T_{max} values all comprised in the 445−455 K range. As in the previous case, the T_{max} values are up-shifted by ∼40 K with respect to that derived from the thermal behavior of the total O1s signal, which shows the inflection point at 410 K (Figure 3c).

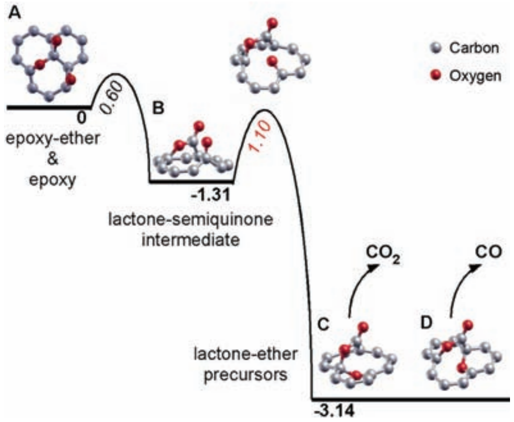

Figure 4. Formation of surface precursors for GO decomposition. Calculated minimum energy path for the formation of the lactone−ether surface precursors from the epoxy−ether pairs assisted by a diffusing neighboring epoxide. Energy differences and barriers are given in eV.

Desorption of CO and CO$_2$ at temperatures as low as 350−400 K, has been observed during the reduction of GO,[10,19] or of C materials exposed to atomic oxygen.[50,51] On the contrary, these species are typically released above 600−670 K[31,30] or even at higher temperatures[32] when C-based materials are oxidized by molecular oxygen and the O atoms are predominantly bonded to graphitic edges or vacancy sites. Here, the low temperature erosion of the graphene network indicates that C atoms are lost via a reaction that benefits from the reservoir of O adatoms diffusing on the basal plane.

Recent calculations have shown that the relevant precursor for GO gasification are ether−lactone pairs.[38] Actually, the high barrier (>1.8 eV) required to dissociate an isolated lactone to molecular CO or CO$_2$ can be reduced to as low as 0.6 eV by the assistance of O adatoms, which diffuse close to the lactone and form the ether−lactone pair.[38] On the basis of the calculated energetics, we propose that the key structure to nucleate the ether−lactone precursor is a pair of two nearest-neighboring O adatoms, whose equilibrium geometry forms an ether−epoxy pair (D in Figure 2). The formation of these structures from epoxide diffusion requires an activation energy (E_a) larger than 1.3 eV and is therefore disfavored over the epoxy recombination and desorption (E_a = 1.13 eV, see Figure 2). However, long graphene exposures to atomic O increase the probability for the adsorption of O adatoms as first neighbors of other epoxy groups already residing on graphene, thus forming stable ether−epoxy pairs.

Once formed, these ether−epoxy pairs are shown to attract the diffusing epoxides (A in Figure 4) and can convert via a two-step reaction mechanism into the lactone−ether precursors, which are more than 3 eV lower in energy than the initial surface structure (epoxy−ether and a diffusing epoxy). The rate-limiting step of the whole process has an activation energy of 1.10 eV (Figure 4), in very good agreement with the value of ~1.20 eV deduced by TPD. This barrier, ultimately governing the CO/CO$_2$ desorption, is comparable to that of epoxy recombination via cycloaddition (1.13 eV) leading to molecular oxygen. The relative position of the ether with respect to the lactone in the lactone−ether precursor (C and D in Figure 4) determines the CO or CO$_2$ products.[38]

The thermal reduction of oxidized graphene will produce molecular oxygen as well as CO and CO$_2$ via competing reaction mechanisms having nevertheless equivalent activation energy barriers. The reduction of graphene oxidized only by isolated epoxy groups or by epoxy−epoxy pairs will produce exclusively molecular oxygen. Higher O coverages will necessarily generate a sizable fraction of nearest-neighbor O adsorbates (ether−epoxy), which easily converts into the lactone−ether pairs, precursors for CO/CO$_2$ desorption. It is worth noticing that once the consumption of the graphene lattice has started, diffusing epoxy groups can bind at vacancies forming additional ethers. Moreover, the thermal decomposition of the lactone−ether pairs leaves C vacancies saturated by ether groups (Figure 4). Both processes, which explain the slightly increasing ether fraction observed during annealing (C3 in Figure 3), favor the formation of additional ether−epoxy pairs.

Despite the lack of molecular oxygen in the TPD spectra of GO,[10,19,21] our study proves that O$_2$ desorption is actually thermodynamically favored provided that the epoxy groups are mobile on the GO basal plane. Actually, the ratios of CO$_2$/O$_2$ and CO/O$_2$ released in the gas phase are directly related to the initial surface density of epoxy species: if the concentration of ethers is enhanced by the presence of defects in the graphene lattice,[29] the rate of the O$_2$ cycloaddition reaction will be damped in favor of competing gasification reactions.

CONCLUSIONS

Our results show that the key factor controlling the onset of lattice damage in GO is the surface density of epoxy species: at low coverage, these undergo reversible desorption, while with increasing coverage they create the precursors for the release of CO/CO$_2$ mixtures. Although chemically synthesized GO contains other functional groups, hydroxyls attached to the basal plane and a variety of species decorating the graphene edges, which will necessarily open other reaction channels, the role identified here for basal plane O atoms in catalyzing the evolution of C at low temperature remains essential.

This opens a new scenario for the thermal reduction of GO. To move forward, novel chemical strategies need to be found to scavenge the epoxy oxygens before they start to diffuse on the surface and trigger the extensive disruption of the graphene network. This will limit the lattice damage to that induced by the removal of O bonded in other functional groups such as ethers and quinones, which desorb as CO and CO$_2$ at higher temperature.

EXPERIMENTAL METHODS

The experiments were performed in the ultra high vacuum chamber (base pressure 8 × 10^{-11} mbar) of the SuperESCA beamline at the Elettra synchrotron radiation facility (Trieste, Italy). The Ir substrate was prepared by cycles of Ar^+ sputtering at 1.5 keV, oxygen treatment between 600 and 1000 K, and flash annealing at 1473 K. Temperatures were measured via a K-type thermocouple spot-welded to the edge of the crystal. The quality of the Ir (111) surface was checked by measuring the Ir4$f_{7/2}$ core level spectrum and by monitoring the LEED pattern. Graphene was grown by ethylene (C_2H_4) pyrolysis in several cycles consisting of saturating the surface at 620 K followed by flash annealing to 1423 K.[41]

Atomic oxygen was produced by a radio frequency plasma source (TECTRA, Gen2) equipped with an ion suppressing grid and an ion trap. The atomic source current and the O$_2$ pressure were kept constant at 20 mA and 8 × 10^{-6} mbar, respectively. The sample was kept at room temperature and exposed to atomic oxygen for increasing time.

Oxidation was performed with the O source facing the back of the sample to minimize any possible damage by energetic ions. Measurements were carried out at oxygen coverage of 0.03 ML ("low O coverage") and 0.25 ML ("high O coverage"), that is, on the graphene surface with a lower oxygen content with respect to GO prepared by wet processing, whose composition varies between $C_8H_2O_3$ to $C_8H_4O_5$.[52] For the thermal desorption experiments, the sample was heated at 0.2 K/s while acquiring O1s and C1s spectra by fast XPS. Alternatively, the sample was heated in steps, and each time high-resolution photoemission spectra were acquired at room temperature. At the end of each experiment, the Ir surface was cleaned, and a fresh graphene layer was prepared.

$Ir4f_{7/2}$, C1s and O1s core level spectra were measured at photon energy of 130, 400, and 650 eV, respectively, with an overall energy resolution ranging from 40 to 150 meV. For each spectrum, the binding energy was calibrated by measuring the Fermi level position of the Ir substrate. The measurements were performed with the photon beam impinging at grazing incidence (70°) while photoelectrons were collected at normal emission angle. The core level spectra were fitted using Doniach−Šùnjić functions convoluted with Gaussians. The oxygen coverage was estimated by evaluating in the C1s spectrum the percentage of C atoms forming single, double, and triple bonds with O atoms and deducing the corresponding amount of adsorbed O.

The TPD data were recorded with a quadrupole mass spectrometer equipped with a "Feulner cup"[53] with a sample-size opening. Before each measurement, the sample was adjusted in front of the cup and was heated with a rate of 2 K/s. To compensate for the difference in ionization efficiency of each molecular species, the measured partial pressures were divided by the corresponding relative sensitivity factors. The TPD curve of CO was corrected for the contribution due to CO_2 cracking.

All simulations were based on the density functional theory (PBE functional) and were performed in the framework of ultrasoft pseudopotentials and plane-waves as implemented in the PWscf code of the Quantum-ESPRESSO package.[54] The energy cutoffs for the electron wave function and augmented charge density were set to 30 and 300 Ry, respectively. Oxygen adsorption and mobility were studied on the freestanding graphene surface, which was modeled with a 5 × 5 supercell together with a 4 × 4 × 1 k-point mesh. Convergence in energy difference and transition states with respect to supercell size, basis set, and k-point sampling was checked to be below 0.02 eV.[38]

Selected calculations were also performed for the O adsorption and mobility on graphene supported by the Ir(111) surface. The metal surface was modeled with a three-layer 9 × 9 slab at the equilibrium lattice constant of bulk Ir (3.895 Å) matching a 10 × 10 graphene sheet. In this case, the k-point sampling was restricted to the Γ point only. All slabs were separated in the perpendicular direction by more than 14 Å of vacuum. As reported in the Supporting Information, the effect of the underlying Ir surface on the mobility and recombination of the epoxy groups is negligible.

Reaction mechanisms and transition barriers were studied with the climbing-image nudged-elastic-band (NEB) method[55] employing between 8 and 10 system replicas. These time-consuming calculations were performed with a 3 × 3 × 1 k-point mesh. Stable structures and transition states were verified by normal-mode analysis. Further details are reported in the Supporting Information.

ASSOCIATED CONTENT

Supporting Information. Full author lists of refs 45 and 53, spectroscopy of the Ir4f core level, further details on the thermal annealing of graphene with high O coverage, additional information concerning O adsorption, mobility, and cycloaddition on Ir(111)-supported graphene, dependence of calculated activation barriers on O coverage, and stability of reaction intermediates. This material is available free of charge via the Internet at http://pubs.acs.org.

AUTHOR INFORMATION

Corresponding Author

rosanna.larciprete@isc.cnr.it; lizzit@elettra.trieste.it

ACKNOWLEDGMENT

S.F. and T.S. acknowledge Regione FVG for funding the project NANOCAT and the ISCRA program of CINECA for computational resources.

REFERENCES

(1) Park, S.; Ruoff, R. S. *Nat. Nanotechnol.* **2009**, *4*, 217–224.

(2) Eda, G.; Chhowalla, M. *Adv. Mater.* **2010**, *22*, 2392–2415.

(3) Loh, K. P.; Bao, Q.; Eda, G.; Chhowalla, M. *Nat. Chem.* **2010**, *2*, 1015–1024.

(4) Dikin, D. A.; Stankovich, S.; Zimney, E. J.; Piner, R. D.; Dommett, G. H. B.; Evmenenko, G.; Nguyen, S. T.; Ruoff, R. S. *Nature* **2007**, *448*, 457–460.

(5) Stankovich, S.; Dikin, D. A.; Piner, R. D.; Kohlhaas, K. A.; Kleinhammes, A.; Jia, Y.; Wu, Y.; Nguyen, S. T.; Ruoff, R. S. *Carbon* **2007**, *45*, 1558–1565.

(6) Kim, J.; Cote, L. J.; Kim, F.; Yuan, W.; Shull, K. R.; Huang, J. *J. Am. Chem. Soc.* **2010**, *132*, 8180–8186.

(7) Gómez-Navarro, C.; Weitz, R. T.; Bittner, A. M.; Scolari, M.; Mews, A.; Burghard, M.; Kern, K. *Nano Lett.* **2007**, *7*, 3499–3503.

(8) Jung, I.; Dikin, D. A.; Piner, R. D.; Ruoff, R. S. *Nano Lett.* **2008**, *8*, 423–487.

(9) Eda, G.; Mattevi, C.; Yamaguchi, H.; Kim, H.; Chhowalla, M. *J. Phys. Chem. C* **2009**, *113*, 15768–15771.

(10) Jung, I.; Field, D. A.; Clark, N. J.; Zhu, Y.; Yang, D.; Piner, R. D.; Stankovich, S.; Dikin, D. A.; Geisler, H.; Ventrice, C. A., Jr.; Ruoff, R. S. *J. Phys. Chem. C* **2009**, *113*, 18480–18486.

(11) Mattevi, C.; Eda, G.; Agnoli, S.; Miller, S.; Mkhoyan, K. A.; Celik, O.; Mastrogiovanni, D.; Granozzi, G.; Garfunkel, E.; Chhowalla, M. *Adv. Funct. Mater.* **2009**, *19*, 2577–2583.

(12) Becerril, H. A.; Mao, J.; Liu, Z.; Stoltenberg, R. M.; Bao, Z.; Chen, Y. *ACS Nano* **2008**, *2*, 463–470.

(13) Schniepp, H. C.; Li, J.-L.; McAllister, M. J.; Sai, H.; Herrera-Alonso, M.; Adamson, D. H.; Prud'homme, R. K.; Car, R.; Saville, D. A.; Aksay, A. *J. Phys. Chem. B* **2006**, *110*, 8535–8539.

(14) Gómez-Navarro, C.; Meyer, J. C.; Sundaram, R. S.; Chuvilin, A.; Kurasch, S.; Burghard, M.; Kern, K.; Kaiser, U. *Nano Lett.* **2010**, *10*, 1144–1148.

(15) Yang, D.; Velamakanni, A.; Bozoklu, G.; Park, S.; Stoller, M.; Piner, R. D.; Stankovich, S.; Jung, I.; Field, D. A.; Ventrice, C. A., Jr.; Ruoff, R. S. *Carbon* **2009**, *47*, 145–152.

(16) Bagri, A.; Mattevi, C.; Acik, M.; Chabal, Y. J.; Chhowalla, M.; Shenoy, V. B. *Nat. Chem.* **2010**, *2*, 581–587.

(17) Li, X.; Wang, H.; Robinson, J. T.; Sanchez, H.; Diankov, G.; Dai, H. *J. Am. Chem. Soc.* **2009**, *131*, 15939–15944.

(18) Moon, I. K.; Lee, J.; Ruoff, R. S.; Lee, H. *Nat. Commun.* **2010**, *1*, 1–6.

(19) McAllister, M. J.; Li, J.-L.; Adamson, D. H.; Schniepp, H. C.; Abdala, A. A.; Liu, J.; Herrera-Alonso, M.; Milius, D. L.; Car, R.; Prud'homme, R. K.; Aksay, I. A. *Chem. Mater.* **2007**, *19*, 4396–4404.

(20) Rourke, J. P.; Pandey, P. A.; Moore, J. J.; Bates, M.; Kinloch, I. A.; Young, R. J.; Wilson, N. R. *Angew. Chem., Int. Ed.* **2011**, *50*, 3173–3177.

(21) Barroso-Bujans, F; Alegria, Á; Colmenero, J. *J. Phys. Chem. C* **2010**, *114*, 21645–21651.

(22) Wei, Z.; Wang, D.; Kim, S.; Kim, S.-Y.; Hu, Y.; Yakes, M. K.; Laracuente, A. R.; Dai, Z.; Marder, S. R.; Berger, C.; King, W. P.; de Heer, W. A.; Sheehan, P. E.; Riedo, E. *Science* **2010**, *328*, 1373–1376.

(23) Zhou, Y.; Bao, Q.; Varghese, B.; Tang, L. A. L.; Tan, C. K.; Sow, C.-H.; Loh, K. P. *Adv. Mater.* **2010**, *22*, 67–71.

(24) Lerf, A.; He, H.; Forster, M.; Klinowski, J. *J. Phys. Chem. B* **1998**, *102*, 4477–4482.

(25) Casabianca, L. B.; Shaibat, M. A.; Cai, W. W.; Park, S.; Piner, R.; Ruoff, S. R.; Ishii, Y. *J. Am. Chem. Soc.* **2010**, *132*, 5672–5676.

(26) Gao, W.; Alemany, L. B.; Ci, L.; Ajayan, P. M. *Nat. Chem.* **2009**, *1*, 403–408.

(27) Cai, W.; Piner, R. D.; Stadermann, F. J.; Park, S.; Shaibat, M. A.; Ishii, Y.; Yang, D.; Velamakanni, A.; An, S. J.; Stoller, M.; An, J.; Chen, D.; Ruoff, R. S. *Science* **2008**, *321*, 1815–1817.

(28) Marchon, B.; Tysoe, W. T.; Carrazza, J.; Heinemann, H.; Somorjai, G. A. *J. Phys. Chem.* **1998**, *92*, 5744–5749.

(29) Carlsson, J. M.; Hanke, F.; Linic, S.; Scheffler, M. *Phys. Rev. Lett.* **2009**, *102*, 166104.

(30) Kelemen, S. R.; Freund, H. *Energy Fuels* **1988**, *2*, 111–118.

(31) Ma, M. C.; Brown, T. C.; Haynes, B. S. *Surf. Sci.* **1993**, *297*, 312–326.

(32) Zhuang, Q.; Kyotani, T.; Tomita, A. *Energy Fuels* **1995**, *9*, 630–634.

(33) He, H.; Klinowski, J.; Forster, M.; Lerf, A. *Chem. Phys. Lett.* **1998**, *287*, 53–56.

(34) Chen, N.; Yang, R. T. *J. Phys. Chem. A* **1998**, *102*, 6348–6356.

(35) Sánchez, A.; Mondragón, F. *J. Phys. Chem. C* **2007**, *111*, 612–617.

(36) Orrego, J. F.; Zapata, F.; Truong, T. T.; Mondragón, F. *J. Phys. Chem. A* **2009**, *113*, 8415–8420.

(37) Radovic, L. R. *J. Am. Chem. Soc.* **2009**, *131*, 17166–75.

(38) Sun, T.; Fabris, S.; Baroni, S. *J. Phys. Chem. C* **2011**, *115*, 4730–4737.

(39) Coraux, J.; N'Diaye, A.; Busse, C.; Michely, T. *Nano Lett.* **2008**, *8*, 565–570.

(40) N'Diaye, A.; Bleikamp, S.; Feibelman, P. J.; Michely, T. *Phys. Rev. Lett.* **2006**, *97*, 215501.

(41) Lacovig, P.; Pozzo, M.; Alfè, D.; Vilmercati, P.; Baraldi, A.; Lizzit, S. *Phys. Rev. Lett.* **2009**, *103*, 166101.

(42) Barinov, A.; Malcioglu, O. B.; Stefano Fabris, S.; Sun, T.; Gregoratti, L.; Dalmiglio, M.; Kiskinova, M. *J. Phys. Chem. C* **2009**, *113*, 9009–9013.

(43) Larciprete, R.; Gardonio, S.; Petaccia, L.; Lizzit, S. *Carbon* **2009**, *47*, 2579–2589.

(44) Vinogradov, N. A.; Schulte, K.; Ng, M. L.; Mikkelsen, A.; Lundgren, E.; Martensson, N.; Preobrajenski, A. B. *J. Phys. Chem. C* **2011**, *115*, 9568–9577.

(45) Balog, R.; et al. *Nat. Mater.* **2010**, *9*, 315–319.

(46) Ivanov, V. P.; Boreskov, G. K.; Savchenko, V. I.; Egelhoff, W. F.; Weinberg, W. H. *Surf. Sci.* **1976**, *61*, 207–220.

(47) Redhead, P. *Vacuum* **1962**, *12*, 203–211.

(48) Cabrera-Sanfelix, P. *J. Phys. Chem. A* **2009**, *113*, 493–498.

(49) Zhang, W.; Carravetta, V.; Li, Z.; Luo, Y.; Yang, J. *J. Chem. Phys.* **2009**, *131*, 244505.

(50) Marsh, H.; O'Hair, T. E.; Wynne-Jones, L. *Carbon* **1969**, *7*, 555–566.

(51) Wicke, B.; Wong, C.; Grady, K. *Combust. Flame* **1986**, *66*, 37–46.

(52) Boukhvalov, D. W.; Katsnelson, M. I. *J. Am. Chem. Soc.* **2008**, *130*, 10697–10701.

(53) Feulner, P.; Menzel, D. *J. Vac. Sci. Technol.* **1980**, *17*, 662–663.

(54) Giannozzi, P.; et al. *J. Phys.: Condens. Matter* **2009**, *21*, 395502.

(55) Jònsson, H.; Mills, G.; Jacobsen, K. W. In *Classical and Quantum Dynamics in Condensed Phase Simulations*; Berne, B. J., Ciccotti, G., Coker, D. F., Eds.; World Scientific: New Jersey, 1998; Chapter 16.